Applied Catalysis B: Environmental 119–120 (2012) 197–206

Contents lists available at SciVerse ScienceDirect

Applied Catalysis B: Environmental

journal homepage: www.elsevier.com/locate/apcatb

# Preparation of the new polyaniline/ZnO nanocomposite and its photocatalytic activity for degradation of methylene blue and malachite green dyes under UV and natural sun lights irradiations

Volkan Eskizeybek[a], Fahriye Sarı[b], Handan Gülce[b,*], Ahmet Gülce[b], Ahmet Avcı[a]

[a] Department of Mechanical Engineering, Selcuk University, Konya 42079, Turkey
[b] Department of Chemical Engineering, Selcuk University, Konya 42079, Turkey

ARTICLE INFO

*Article history:*
Received 6 January 2012
Received in revised form 24 February 2012
Accepted 28 February 2012
Available online 6 March 2012

*Keywords:*
Polyaniline
ZnO
Polyaniline/ZnO nanocomposite
Photocatalysis
Natural sunlight
UV light

ABSTRACT

A new polyaniline (PANI) homopolymer and PANI/ZnO nanocomposite have been successfully synthesized in aqueous diethylene glycol solution medium via the chemical oxidative polymerization of aniline. Scanning electron microscopy, transmission electron microscopy, X-ray diffraction, FTIR spectra, UV–vis spectroscopy measurements were used to characterize the resulting PANI homopolymer and PANI/ZnO nanocomposite photocatalysts. The photocatalytic activities of PANI homopolymer and PANI/ZnO nanocomposites were investigated by the degradation of methylene blue (MB) and malachite green (MG) dyes in aqueous medium under natural sunlight and UV light irradiation and the efficiency of the catalysts have been discussed in detail. Results indicate that the addition of the ZnO nanoparticles to the PANI homopolymer enhance the photocatalytic efficiency under natural sunlight irradiation and a little amount of PANI/ZnO nanocomposite photocatalyst (0.4 g/L) degrades both of the dye solutions (MB or MG) with 99% efficiency after 5 h of irradiation under natural sunlight.



## 1. Introduction

Nowadays, the growing population has led to the increase mainly contamination of surface and ground water. Organic dyes used in textile and food industries are their important sources of the environmental contaminations due to their non-bio degradability and high toxicity to aquatic creatures and carcinogenic effects on humans. Malachite green (MG) (Color Index No. 42000), also called basic green 4 or victoria green B, having IUPAC name 4-[(4-dimethylaminophenyl)-phenyl-methyl]-*N*,*N*-dimethylaniline with chemical formula $C_{23}H_{25}N_2Cl$, is a green crystal powder with a metallic luster, highly soluble in water and ethanol with blue-green solutions. [1]. Methylene blue (MB) (Color Index No. 52015) is a heterocyclic aromatic chemical compound having IUPAC name 3,7-bis(dimethylamino)-phenothiazin-5-ium chloride with the molecular formula $C_{16}H_{18}N_3SCl$. It has many uses in a range of different fields, such as biology and chemistry. At room temperature it appears as a solid, odorless, dark green powder that yields a blue solution when dissolved in water. The International Nonproprietary Name (INN) of MB is methylthionium chloride. It is a highly toxic chemical primarily used as a dye as like as MG [2–4]. In order to decrease damage caused by organic dye pollution to environment and humans, the use of photocatalyst to degrade organic compounds in contaminated air or water or to convert them into harmless chemicals has been extensively studied. In this manner, metal oxide nanoparticles such as ZnO [5], $TiO_2$ [6], etc. [7–9] has been widely used to degrade non-biodegradable dyes by photocatalytical routes. Therefore, the researches focused on increasing degradation rate of pollutants by combining inorganic materials with conductive polymers to realize synergetic and complementary behaviors between the polymer and inorganic materials [10–13]. Many conducting polymers are known as good hole conducting materials [14,15]. These conductive polymers act as a stabilizer or surface capping agents when combined with metals or semiconductor nanoparticles [16–19]. ZnO is a wide band gap semiconductor (3.37 eV) with a 60 meV exciton binding energy, which permits laser emission at room temperature [20]. This large band gap is suitable for the use of ZnO to collect high-energy photons (UV light) [21]. Due to these properties, it has a potential for wide range of optical and electronic applications such as photovoltaic devices, solar cells, transducers, etc. [22–24]. Conducting polyaniline (PANI) is one of the promising polymers studied polymer due to high conductivity, simple synthesis procedure, good environmental stability [25,26] and a large variety applications such as in electro-chromic devices, light emitting diodes, corrosion-protecting paint and electrostatic discharge protection [27–29].

* Corresponding author at: Selcuk University, Department of Chemical Engineering, Alaeddin Keykubat Campus, Selcuklu, Konya, 42079, Turkey.
Tel.: +90 332 2232071; fax: +90 332 2410651.
*E-mail address:* hgulce@selcuk.edu.tr (H. Gülce).

0926-3373/$ – see front matter © 2012 Elsevier B.V. All rights reserved.
doi:10.1016/j.apcatb.2012.02.034

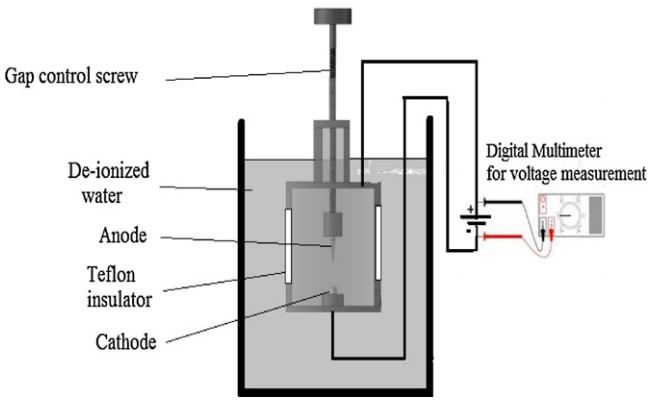


**Fig. 1.** Schematic view of the arc-discharge apparatus.

There are several reports focused on increasing ultraviolet emission and photocatalytic activity of ZnO nanostructures combined with polyaniline conductive polymer [7,30].

The aim of this study was to investigate the comparative photocatalytical activity of the new PANI homopolymer and PANI/ZnO nanocomposite under both UV and natural sun light irradiation for the degradation of MB and MG. For this, a new PANI homopolymer and PANI/ZnO nanocomposites were synthesized in aqueous diethylene glycol solution via chemical oxidation of aniline in the present work for the first time. The surface structure and morphology of the PANI homopolymer and PANI/ZnO nanocomposites were characterized by scanning electron microscopy (SEM), transmission electron microscopy (TEM), X-ray diffraction (XRD), FTIR spectra (FT-IR), UV–vis spectroscopy (UV–vis) analysis. In addition, the photocatalytical activities of the synthesized PANI homopolymer and PANI/ZnO nanocomposites were characterized by monitoring the degradation of methylene blue (MB) and malachite green (MG) dyes under irradiation with natural sunlight and UV light. The influences of organic dye type, light source, irradiation time, photocatalyst amount and reusing of photocatalysts on the photocatalytic activity were investigated.

## 2. Experimental

### 2.1. Materials

Monomer aniline (Merck) was distilled under reduced pressure and stored in dark below 4 °C. High purity Zn rods (Alfa Aesar, 99.99%) were used as electrodes to synthesize ZnO nanoparticles via arc discharge method in de-ionized water. All other reagents, including ammonium peroxydisulphate (APS), diethylene glycol, methylene blue (MB) and malachite green (MG), were supplied by Merck. Bi-distilled water was used throughout the experimental work. All reagents were of analytical grade and used without further purification.

### 2.2. Synthesis of ZnO nanoparticles

Arc-discharge method submerged in de-ionized water was used to synthesize ZnO nanoparticles. The arc discharge apparatus consists of two Zn electrodes as anode and cathode as seen Fig. 1. The arc discharge was initiated in the de-ionized water by touching the anode to the cathode and then the gap between the electrodes was controlled by hand at about 1 mm to maintain stable arc discharge. Discharge voltage between electrodes was measured and tried to keep constant by controlling the gap. The applied arc current was decided as 50 A after several experiments as an optimum current to produce large scale and effective nanoparticles. The arc current was supplied by a direct current (dc) welding power supply. During arc-discharge the temperature between electrodes can increase more than 5000 °K. Arc discharge was continued for 3 min. The resulted particles were kept at room temperature to complete settling at the bottom of the reaction vessel for 24 h. The settled particles were collected carefully by pouring the products into a 500 ml beaker by decantation of almost all the suspension. The collected particles were washed with de-ionized water and absolute ethanol to remove the ions possibly in the final product for five times dried at 40 °C under vacuum for 24 h.

### 2.3. Synthesis of PANI polymer and PANI/ZnO nanocomposite

PANI homopolymer was synthesized by polymerization of aniline in aqueous diethylene glycol solution medium by chemical oxidation. 0.4 M aniline monomer solution was prepared with aqueous 1 M diethylene glycol. Meanwhile, 0.4 M APS was dissolved in aqueous 1 M diethylene glycol solution and 25 mL of this solution was added to 25 mL of the aniline monomer solution. The resulted solution was mixed for 1 min by using magnetic stirrer, subsequently the resulted solution was kept 2 h under room temperature conditions for polymerization. After polymerization, the dark green colored emeraldine salt of PANI was washed with de-ionized water and finally the filtered polymer was dried at 40 °C under vacuum for 24 h.

PANI/ZnO nanocomposites were prepared by the same way of PANI in the presence of ZnO nanoparticles. 8.8 mg ZnO nanoparticles were dispersed into aqueous 1 M diethylene glycol solution via tip sonication for 10 min to obtain a uniform suspension. 0.4 M aniline and 0.4 M APS solutions prepared with 1 M diethylene glycol were added into ZnO/diethylene glycol suspension. The resulted solution was mixed for 1 min by using magnetic stirrer. Then the mixture was allowed to polymerize under room temperature without stirring for 2 h. The PANI/ZnO nanocomposite was filtered and washed with large amount of de-ionized water after polymerization. Finally, the filtered nanocomposite was dried at 40 °C under vacuum for 24 h.

### 2.4. Characterization

X-ray diffraction (XRD) analysis was carried out by Shimadzu XRD-6000 X-ray diffractometer using Cu $K_\alpha$ radiation ($\lambda$ = 0.15418 nm) the operating conditions were 40 kV and 30 mA in the scanning range from 10° to 70° at rate of 2°/min. The morphology of the synthesized products was carried out using a JEOL/JSM-6335F-EDS SEM. The TEM images of the ZnO nanoparticles were performed using JEOL 2100 HRTEM at 300 kV. The optical absorption spectra of all the samples were obtained using an Ocean Optics HR4000 UV–visible spectrophotometer and the FTIR spectra of all materials were recorded by a Perkin Elmer 1725 spectrophotometer.

### 2.5. Measurement of photocatalytic activities

The photocatalytical activity of PANI and PANI/ZnO nanocomposite were performed using MB and MG dyes as degraded materials in quartz tubes under UV light and natural sunlight irradiation. The UV-C tube lamp (15 W, length 41 cm, diameter 2.5 cm), model G15T8 (Philips, Holland) was used as the irradiation source ($\lambda$ = 254 nm) located in a light infiltrated chamber. 2.5 mL dye solution (MB or MG) was mixed with desired amount catalysts. Before irradiation, suspension was stirred magnetically for 30 min in dark conditions until adsorption–desorption equilibrium was established. And then, the suspensions were irradiated by light sources without stirring. Under natural sunlight investigations, all experiments were done inside laboratory in an open atmosphere

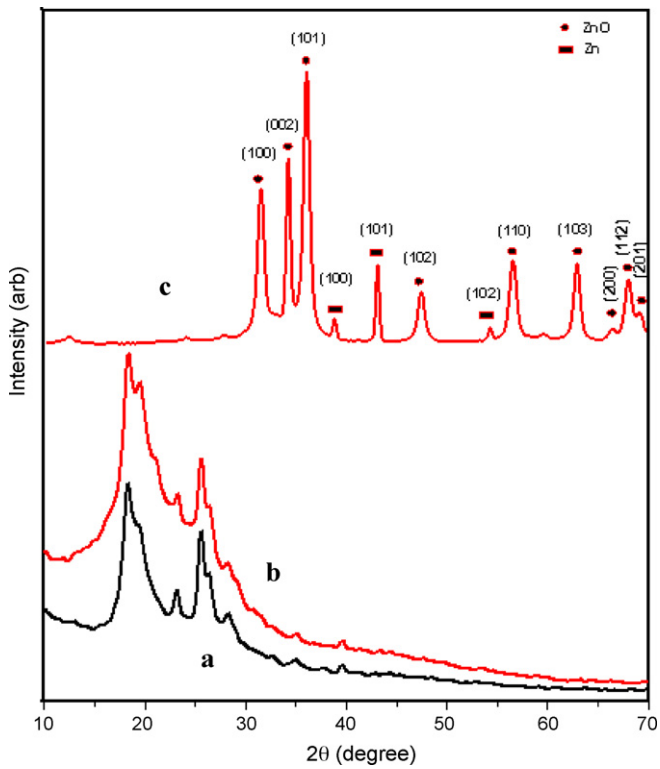


**Fig. 2.** The XRD patterns (**a**) PANI, (**b**) PANI/ZnO nanocomposite and (**c**) ZnO nanoparticle.

between 10.00 am and 3.00 pm in the months of June and July as applied before by the literature [52]. The catalytic degradation of organic dyes was investigated at room temperature in the presence/absence of different catalysts under irradiation/dark for given times.

The concentrations of the dyes for each sample were analyzed by using UV–vis spectroscopy method and absorptions of the dyes at characteristic wavelength were measured. The concentrations of the dyes were calculated by calibration curves. The decolorization efficiencies of the dyes are estimated by the following equation;

$$\text{Degradation}\,(\%) = \frac{C_o - C}{C_o} \times 100 \qquad (1)$$

where $C_o$ represents the concentration of the dye before illumination, $C$ denotes the concentration of dye after a certain irradiation time, respectively.

## 3. Results and discussion

### 3.1. Structure and morphology

The XRD patterns of PANI, PANI/ZnO nanocomposite and ZnO nanoparticles were shown in Fig. 2. In the pattern of the PANI (Fig. 2a), four peaks can be observed in the region of $2\theta = 15–30^\circ$ where maximum peak is around $2\theta = 18.5^\circ$ and ascribed to the periodicity parallel and perpendicular polymer (PANI) chain. The peak at $2\theta = 20^\circ$ also represents the characteristic distance between the ring planes of benzene rings in adjacent chains or the close contact inter-chain distance [31]. In addition, the peak centered at $2\theta = 25^\circ$ may be assigned to the scattering from PANI chains at interplanar spacing [32,33] and indicate that the PANI had also some degree of crystallinity. The XRD pattern of the PANI/ZnO nanocomposite (Fig. 2b) shows the peaks with corresponding PANI and no additional characteristic peaks of ZnO nanoparticles were appeared. This result may be attributed to low ZnO/Aniline molar ratio and

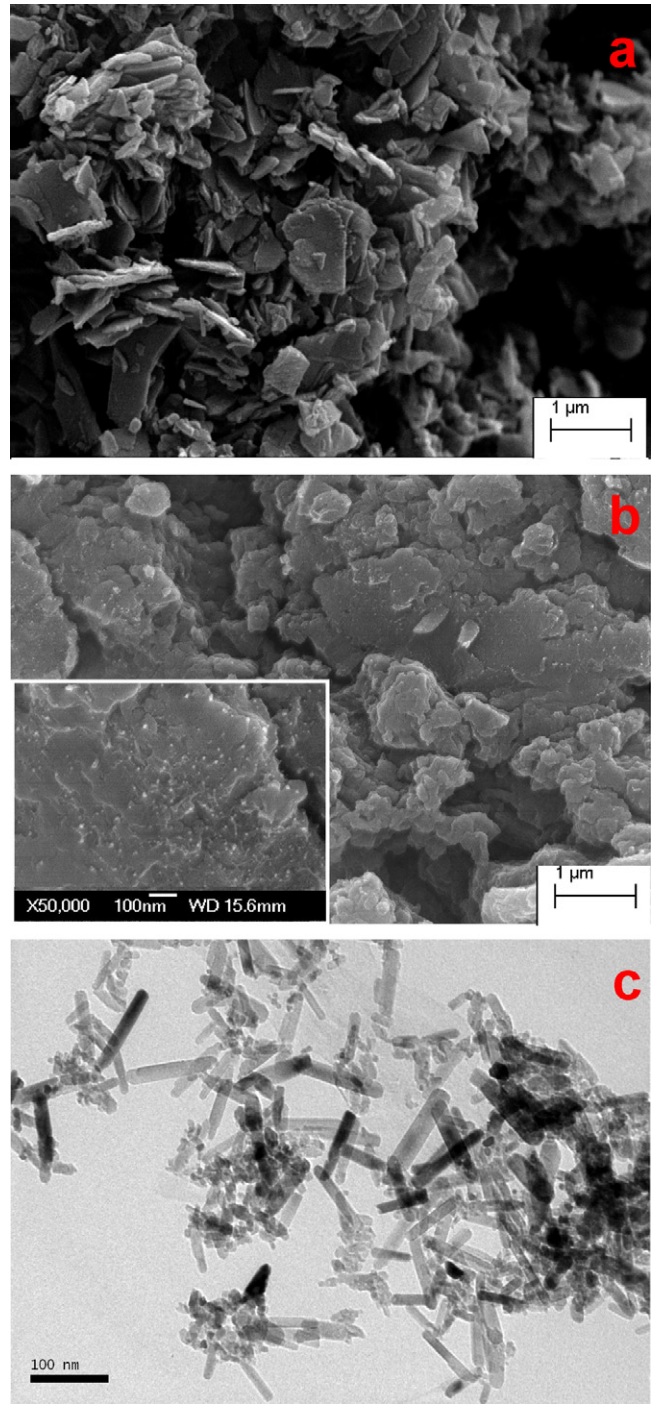


**Fig. 3.** (**a**) SEM image of PANI, (**b**) SEM image of PANI/0.01 M ZnO nanocomposite and (**c**) TEM image of bare ZnO nanoparticles.

polymerization degree of the PANI. The XRD pattern of the ZnO nanoparticles was represented in Fig. 2c. It can be seen from the figure that the XRD pattern shows two kinds of materials' peaks. Once is assigned to ZnO and the other is metallic Zn. All of the labeled ZnO peaks assigned to the crystalline zinc oxide phase with the hexagonal wurzite structure with the lattice parameters $a = 0.324$ nm and $c = 0.519$ nm (joined powder diffraction files JPDS No.30-1451). This peak broadening indicates the nanometer scaled grain size.

Morphologies of synthesized PANI and PANI/ZnO nanocomposites were investigated by SEM technique. Fig. 3 shows the SEM images of PANI and PANI/ZnO nanocomposites and TEM image of the ZnO nanoparticles synthesized via arc discharge method.

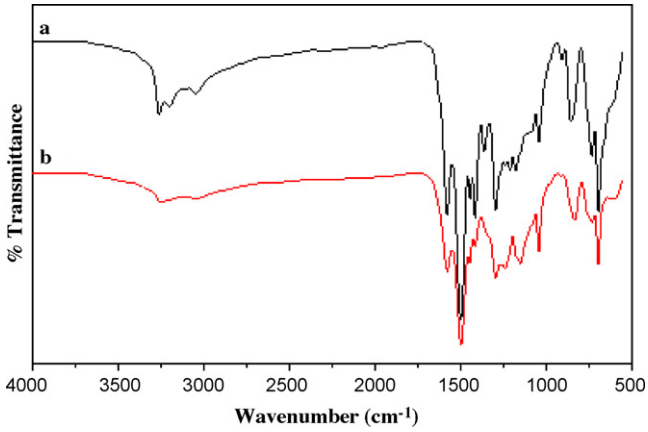


**Fig. 4.** FTIR spectra of (**a**) the PANI polymer and (**b**) PANI/ZnO nanocomposite.

The PANI displays micron sized irregular sheet-like morphology as seen in Fig. 3a. For the PANI/ZnO nanocomposite, ZnO nanoparticles are dispersed uniformly in the PANI matrix as seen in Fig. 3b. As seen at the inset of the figure (marked with rectangle), the ZnO nanoparticles are coated by the PANI polymer matrix tightly and results as a core–shell structure. The PANI chains enclose the ZnO nanoparticles and the nanocomposite particles grow as multiparticles. The same observations can be found in the literature [34,32,35]. In this manner, it is hard to observe ZnO nanoparticles in the PANI matrix at low magnifications. This observation supports the reason why hexagonal wurzite ZnO peaks were not displayed in the XRD spectrum of the PANI/ZnO nanocomposite. We anticipate that the hexagonal wurzite ZnO peaks are suppressed by the high intensity PANI polymer peaks. TEM investigations were carried out to understand morphology and structure of the synthesized ZnO nanoparticles. TEM analysis reveals that the ZnO nanoparticles are almost in nanorod form as seen in Fig. 3c. The ZnO nanorods have diameters ranging between 10 and 30 nm and in the length ranging between 50 and 100 nm. Similar result was obtained by Fang et al. [36]. Furthermore, some nanorods like nanoparticles with diameters around 10 nm are also observed.

FTIR analysis was also carried out to understand structure of the PANI and PANI/ZnO nanocomposite. As seen in Fig. 4a, the PANI exhibits characteristic peaks around 3225 $cm^{-1}$ attributed to N–H stretching mode [37], the C=N and C=C stretching of quinoid and benzenoid units occur at 1576 $cm^{-1}$ and 1490 $cm^{-1}$ respectively. In addition, the band at 1287 $cm^{-1}$ is assigned to the C–N stretching of benzenoid while the band at 1100 $cm^{-1}$ is due to the quinoid unit of PANI. The presence of the benzenoid and quinoid units is evidence of the emeraldine form of PANI. The FTIR spectrum of the PANI/ZnO nanocomposite (Fig. 4b) represents the same characteristic peaks with the PANI. However, the corresponding peaks are shifted to the lower wave numbers, besides their intensities are changed after the ZnO nanoparticles addition. The peaks of the PANI around 1576 $cm^{-1}$, 1490 $cm^{-1}$ and 1041 $cm^{-1}$ are shifted to 1567 $cm^{-1}$, 1480 $cm^{-1}$ and 1031 $cm^{-1}$, respectively. These shifts of characteristic peaks of the PANI may be the result of the interactions between the PANI chains and ZnO nanoparticles which affect the electron densities and bond energies of the PANI [38,39]. The shifting to the lower wave numbers may be shows the increasing the electron density of PANI chains.

### 3.2. Optical property

The UV–vis spectra of the ZnO nanoparticles, the PANI and the PANI/ZnO nanocomposites were exhibited in Fig. 5. The absorption spectrum of the ZnO nanoparticles (Fig. 5a) presents a sharp

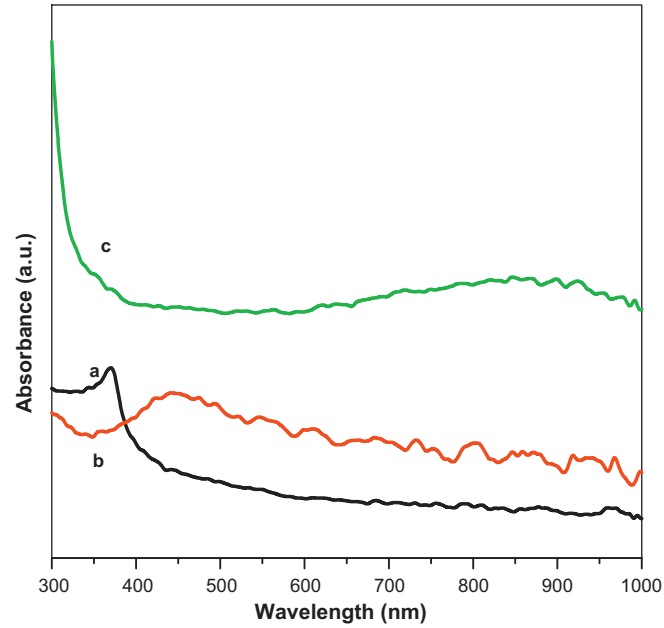


**Fig. 5.** UV–vis spectra of (**a**) ZnO nanoparticles and (**b**) PANI (**c**) PANI/ZnO nanocomposite.

absorption peak around 378 nm which is the characteristic single peak of hexagonal ZnO nanoparticles. As reported previously by some researchers doped forms of PANI show usually three characteristic absorption bands at 320–360, 400–450 and 740–950 nm [40]. The first absorption band arises from $\pi$–$\pi^*$ electron transition within benzenoid segments [41]. The second and third absorption bands are related to doping level and formation of polarons (quinoid segments), respectively. Similarly, the PANI has unseparated broad bands around 350–450 nm as shown in Fig. 5b. The other characteristic peaks which corresponding to doping level of the PANI cannot be seen for the PANI. This result may be attributed to the diethylene glycol used solvent during chemical polymerization of the PANI polymer. In the literature, the absorption peaks of PANI between 700 and 800 nm with high intensities were related with the presence acidic solvents used as medium during polymerization of aniline [42]. The absorption spectrum of the PANI/ZnO nanocomposite was exhibited in Fig. 5c. Two main dissimilarities can be seen for the absorption spectrum of the PANI/ZnO nanocomposite when compared with the absorption spectrum of the PANI. The broad peak around 450 nm is disappeared while a broad peak appears from 700 to 800 nm. This result indicates that the doping level of the PANI polymer is increased by adding ZnO nanoparticles. Furthermore, the characteristic peak of ZnO nanoparticles around 378 nm cannot be observed in PANI/ZnO nanocomposite's absorption spectrum as like as XRD spectrum PANI/ZnO nanocomposite.

The nature of the optical band gap can be determined using the fundamental absorption, which corresponds to electron excitation from valence band to conduction band. Direct absorption band gaps of the ZnO nanoparticles and PANI can be obtained by conforming the absorption data to the following equation [49]; $\alpha h\nu = B(h\nu - Eg)^n$, where $\alpha$ is the absorption coefficient, $h\nu$ is the photon energy, $E_g$ is the optical band gap of the material, $B$ is the material constant and $n$ is either 2 for direct transition or ½ for an indirect transition. Therefore the optical band gaps of ZnO nanoparticles and PANI for the absorption edge can be determined by extrapolating the straight portion of the curve $(\alpha h\nu)^2$ versus $h\nu$ when $\alpha = 0$. The calculated $E$ values were 3.3 eV and 2.81 eV for ZnO nanoparticles and PANI, respectively.

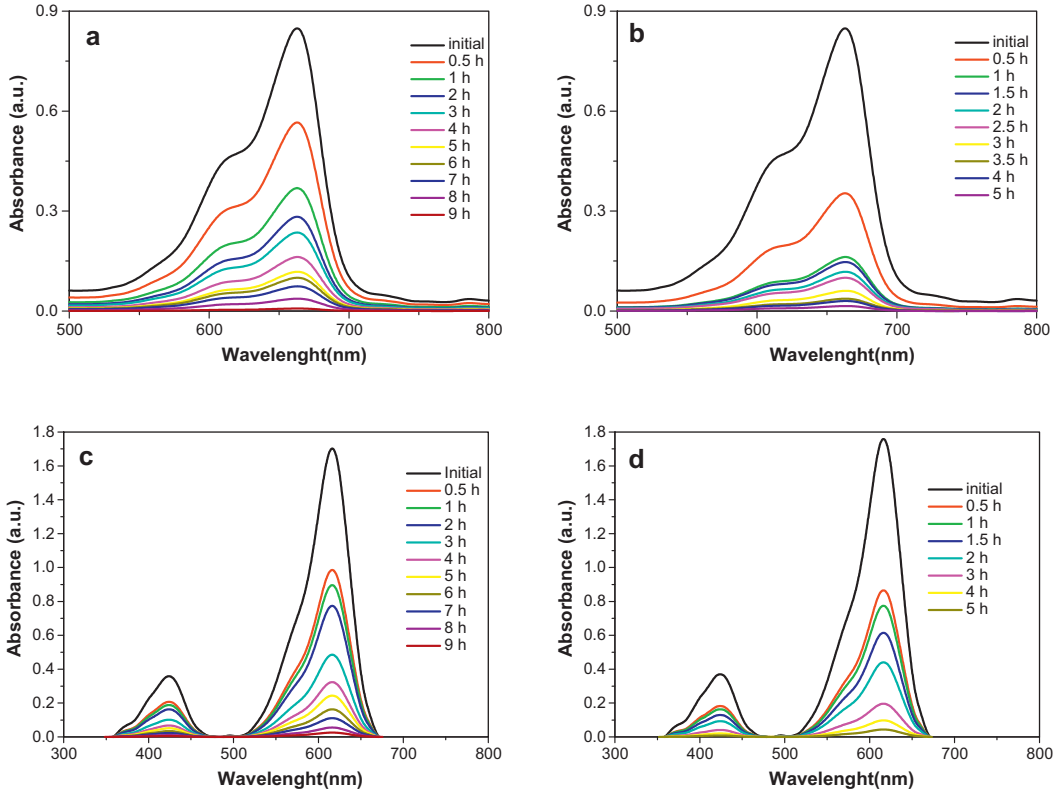


**Fig. 6.** UV–vis absorption spectra of MB and MG dyes PANI/ZnO nanocomposites for different irradiation times under (**a**) UV light irradiation of MB, (**b**) natural sunlight irradiation of MB, (**c**) UV light irradiation of MG and (**d**) sunlight irradiation of MG (catalyst concentration: 0.4 mg/mL; initial concentration of dyes: $1 \times 10^{-5}$ M).

### 3.3. Photocatalytic activity

#### 3.3.1. Photocatalytic degradation of MB and MG under UV and sun light illuminations

The photocatalytic degradation of MB and MG dyes in the presence of the PANI/ZnO nanocomposite as catalyst under different light source irradiations were investigated. The change in optical absorption spectra of MB and MG dyes by PANI/ZnO nanocomposites catalyst under UV or natural sunlight irradiation for different time intervals were shown in Fig. 6. The decrease of the absorption band intensities of the dyes indicated that dyes have been degraded by PANI/ZnO nanocomposites photocatalyst. As can be seen this figure, the disappearance of the characteristic band of MB dye at 664 nm after 9 h under UV light irradiation indicates that MB has been degraded completely by PANI/ZnO nanocomposite (Fig. 6a). On the other hand, the characteristic peak of the MB dye solution decreases suddenly after 30 min exposure time under natural sunlight irradiation (Fig. 6b). Furthermore, when the MB dye solution was exposed to the natural sunlight for 6 h, the decolorization efficiency the MB dye is around 94% in the presence of the PANI/ZnO nanocomposite. By the same way, the change in optical absorption spectra of the MG dye by PANI/ZnO nanocomposite under UV and natural sunlight irradiations for different time intervals are also investigated. In Fig. 6c, it can be seen that the disappearance of the MG dye's characteristic peaks around 423 and 615 nm indicates that the MG dye has been decolorizated by PANI/ZnO nanocomposite. The decolorization efficiency of the MG dye is around 95% after 10 h under UV light irradiation. On the other hand, when the MG dye solution was exposed to the sunlight for 5 h, the decolorization efficiency the MB dye is around 98% in the presence of the PANI/ZnO nanocomposite. After these investigations, it is clear that the PANI/ZnO nanocomposite is more efficient under natural sunlight conditions for the decolorization of the both MB and MG dyes.

Fig. 7 shows the variation in decolorizing efficiency versus irradiation time for the MB and MG dyes solutions in the presence of the ZnO nanoparticles, the PANI and the PANI/ZnO nanocomposites. In order to investigate the effect of irradiation on the catalyst/dye interaction, three sets of experiments were carried out. The first set involves the degradation of the dyes in the presence of UV or natural sunlight without catalyst. No significant changes were observed in absorption spectrum of dyes, the decolorization efficiency rate of the MB is less than 2% after 5 h irradiation under UV or natural sunlight (Fig. 7a and b). The decolorization efficiency of MG without catalyst were also investigated and it was found that it is less than 7% and 5% after 5 h irradiation under UV or natural sunlight, respectively (Fig. 7c and d). The results showed that the photolysis of the dyes is negligible. In the second set, the experiments were also realized in dark condition to understand the effect of the light source when the catalyst material added into the dyes. As seen, the decolorization efficiencies are 18% and 20% for MB and MG dyes respectively under dark conditions in the presence of the PANI/ZnO nanocomposite used as catalyst due to adsorption mechanism. The third set of experiments was performed to study the effect of UV or natural sunlight irradiation on the catalyst/dye interaction. The decolorization efficiencies of the dyes are very higher than corresponding dark conditions in the presence of the PANI/ZnO nanocomposite under illumination. The results show that the PANI/ZnO nanocomposite exhibit good photocatalytic performance.

The experimental results are summarized in Table 1. It is clear that almost complete degradation of the MB and MG dyes has been achieved in 5 h natural sunlight irradiation using PANI/ZnO nanocomposite as photocatalyst. The decolorization efficiency of the PANI is lower than the PANI/ZnO nanocomposite in same conditions. It is obvious that the ZnO nanoparticles play important role to increase photocatalytic activity of the PANI matrix, especially the decolorization efficiency of the PANI

**Table 1**
Degradation (%) of MB and MG dyes in the presence of the PANI and the PANI/ZnO nanocomposite photocatalysts after 5 h illumination under different light source irradiations (catalyst concentration: 0.4 mg/mL; initial concentration of dyes: $1 \times 10^{-5}$ M).

| | PANI | | | PANI/ZnO | | |
|---|---|---|---|---|---|---|
| | UV | Sunlight | Dark | UV | Sunlight | Dark |
| Degradation (%) of MB | 28 | 85 | 10 | 79 | 97 | 18 |
| Degradation (%) of MG | 34 | 81 | 10 | 89 | 99 | 20 |

increased almost up to 3 times under UV light irradiation for both dyes.

In general, the kinetics of photocatalytic degradation of organic pollutants on the semiconducting oxide has been established and can be described well by the apparent first order reaction $\ln(C_0/C_t) = k_{app}t$, where $k_{app}$ is the apparent rate constant, $C_0$ is the concentrations of dyes after darkness adsorption for 30 min and $C_t$ is the concentration of dyes at time $t$. Fig. 8 shows the relationship between illumination time and the degradation rate of dyes for UV and natural sunlight illumination. The linear correlation of the plots of $\ln(C_0/C_t)$ versus time suggested a pseudo first-order reaction for the both dyes.

The photocatalytic activity of synthesized nanocomposite under UV light and natural sunlight can be evaluated by comparing the apparent rate constants ($k_{app}$) listed in Table 2. From Table 2, it can be seen that the photocatalytic activities of the PANI and the PANI/ZnO nanocomposite catalysts under natural sunlight irradiation are higher than that of under UV light illumination.

Our studies indicated that, the synthesized PANI/ZnO nanocomposite is more effective on the decolorization of MB under the same conditions to the literature [10] while used photocatalyst content is five times less than corresponding literature for the same conditions. In addition, the PANI/ZnO nanocomposite has been compared other types of photocatalysts like PANI/$TiO_2$ [1,32,43,44] and results indicated that the PANI/ZnO nanocomposite system is more effective when compared those of the PANI/$TiO_2$ photocatalysts under natural sunlight irradiation.

The basic mechanism of photocatalysis over irradiated ZnO was well established [10,34,43,44]. ZnO nanoparticles are irradiated with UV light to generate electron–hole pairs, which can react with water to yield hydroxyl and super-oxide radicals to oxidize and mineralize the organic and inorganic molecules. However, the band gap of ZnO is 3.3 eV, only UV light can excite the ZnO nanoparticles to generate electron–hole pairs. Energy of UV light is so little in the solar photons (only 3–5%) that poor photocatalytic efficiency presents under sunlight. One solution to overcome this shortcoming is to use a dye with narrow band gap as a sensitizer, so as to enhance the photocatalytic efficiency of ZnO. PANI has a band gap of 2.81 eV, which is narrower than 3.3 eV of ZnO, showing absorption in the region of visible light. Hence, it may function as a photo sensitizer to ZnO [45]. As can be seen in Fig. 5 PANI has high absorption in the visible light region while the ZnO nanoparticles have high absorption intensity in the UV range. On the other hand, the PANI/ZnO nanocomposite has absorption either in the UV range or in the visible light region when compared those of the PANI and the ZnO nanoparticles. Hence, the PANI/ZnO nanocomposite can be excited to produce more electron hole pairs under natural sunlight irradiation which could result efficient

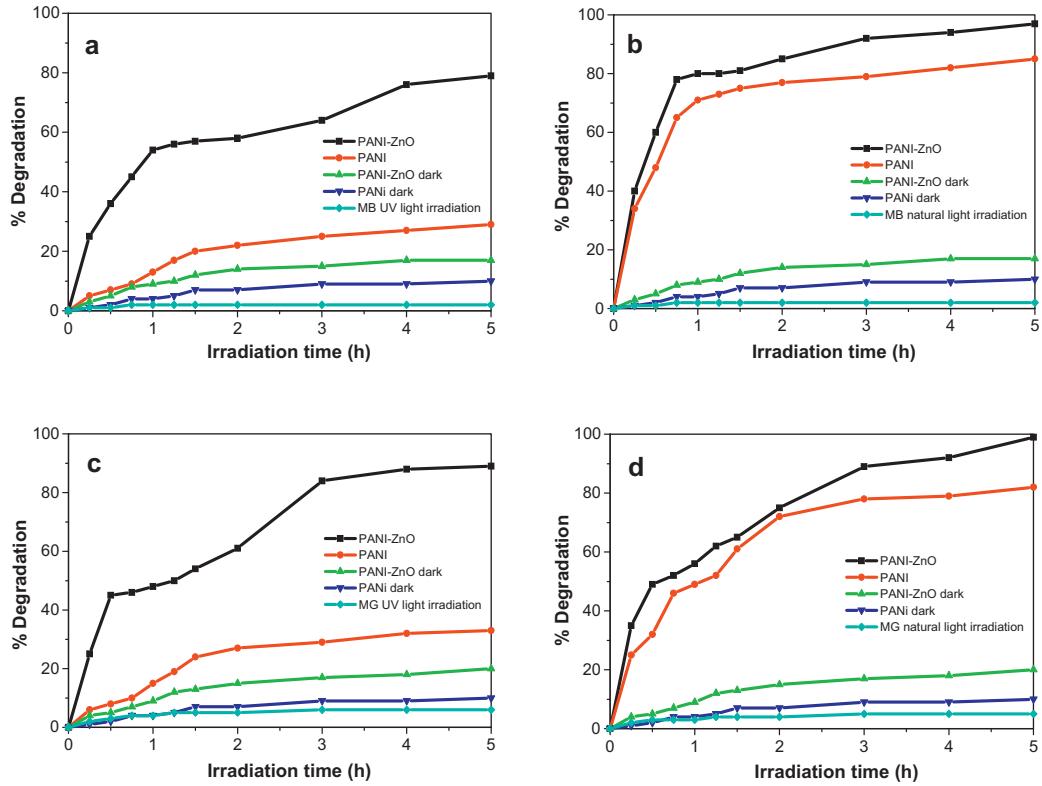


**Fig. 7.** Extend of decomposition of the MB and MG dyes with respect to time intervals over PANI, PANI/ZnO nanocomposite and ZnO nanoparticles under (**a**) UV light irradiation of MB, (**b**) natural sunlight irradiation of MB, (**c**) UV light irradiation of MG and (**d**) natural sunlight irradiation of MG (catalyst concentration: 0.4 mg/mL; initial concentration of dyes: $1 \times 10^{-5}$ M).

**Table 2**
Apparent rate constants ($k_{app}$) of dyes degradation and linear regression coefficients from plot of $\ln(C_o/C_t) = k_{app}t$ for different dye concentrations (catalyst concentration: 0.4 mg/mL).

| | | PANI | | | | PANI/ZnO | | | |
|---|---|---|---|---|---|---|---|---|---|
| | | UV | | Sunlight | | UV | | Sunlight | |
| | | $k_{app}$ (min$^{-1}$) | $R^2$ | $k_{app}$ (min$^{-1}$) | $R^2$ | $k_{app}$ (min$^{-1}$) | $R^2$ | $k_{app}$ (min$^{-1}$)$^2$ | $R^2$ |
| MB | $10^{-5}$ M | 0.00237 | 0.99 | 0.01873 | 0.98 | 0.011 | 0.98 | 0.02405 | 0.95 |
| | $10^{-6}$ M | 0.00618 | 0.99 | 0.03669 | 0.99 | 0.01862 | 0.96 | 0.03224 | 0.95 |
| MG | $10^{-5}$ M | 0.00271 | 0.99 | 0.01009 | 0.97 | 0.00914 | 0.90 | 0.01219 | 0.95 |
| | $10^{-6}$ M | 0.0066 | 0.99 | 0.02427 | 0.99 | 0.02200 | 0.96 | 0.02849 | 0.97 |

photocatalytic activity. When PANI/ZnO nanocomposite is irradiated under natural sunlight, both ZnO and PANI absorb the photons at their interface, and then charge separation occurs at the interface. This is because the conduction band of ZnO and the lowest unoccupied molecular orbital level of the PANI are well matched for the charge transfer [46]. The electrons generated by conducting PANI can be transferred to the conduction band of ZnO, enhancing the charge separation and in turn promoting the photocatalytic ability of the photocatalyst. The synergetic effect between ZnO and PANI on the photocatalytic degradation of dyes exists clearly for the PANI/ZnO nanocomposite.

Since the existence of the MB and MG dyes during photocatalysis, a dye sensitized photocatalytic process may also be able to operate, in which case the adsorbed dye molecules are excited by solar light and thus act as photosensitizers [50,51]. The first step in the dye sensitized degradation reaction is the adsorption of the dye (MB or MG) on the surface of the nanocomposite.

$$\text{PANI/ZnO} + \text{D} \rightarrow \text{PANI/ZnO} - \text{D}_{\text{ads}} \tag{2}$$

The second step of this mechanism is excitation of the dye by visible light, and the formation of the excited state dye species ($D^*_{ads}$).

$$\text{PANI/ZnO} - \text{D}_{\text{ads}} \rightarrow \text{PANI/ZnO} - \text{D}^*_{\text{ads}} \tag{3}$$

Photoexcitation of the dye is followed by the electron transfer reaction, which plays a vital role in the initiation of the reactions involving the degradation of the organic dye. This enhances the photo excited electron transfer from solar light sensitized dye molecule to the conduction band of ZnO and subsequently increase the electron transfer to the adsorbed oxygen. The electron transfer is accompanied by the concomitant formation of the dye radical cation ($D^{+\bullet}_{ads}$). In addition to the degradation of the dye by the usual ZnO sensitization mechanism, the dye molecules are also degraded by the super oxide radicals produced by dye sensitization mechanism (Eqs. (4–6)).

$$\text{PANI/ZnO} - \text{D}^*_{\text{ads}} \rightarrow \text{PANI/ZnO} - \text{D}^{+\bullet}_{\text{ads}} + e^-_{CB} \tag{4}$$

$$e^-_{CB} + \text{O}_2 \rightarrow \text{O}_2^{\bullet -} \tag{5}$$

$$\text{D}^{+\bullet}_{\text{ads}} + \frac{\text{O}_2}{\text{O}_2^{o-}} \rightarrow\rightarrow \text{degradation products} \tag{6}$$

$CO_2$ gas generation was also observed during degradation reaction of the dyes with PANI or PANI/ZnO nanocomposite. $CO_2$ gas was identified by saturated $BaCl_2$ solution test via white $BaCO_3$ precipitate formation.

### 3.3.2. Effect of photocatalyst dosages

In order to optimize the photocatalyst suspension concentration, the effect of photocatalyst dosages on the degradation of the dyes in water was investigated under UV light irradiation. The experiments were carried out at a fixed concentration of dye ($1 \times 10^{-5}$ M) and fixed degradation time (5 h). The effect of the photocatalyst loading on decolorization rate of the dyes was examined by varying photocatalyst concentration from 0.2 mg/mL to 1.6 mg/mL of the dye solution. The results were shown in Fig. 9. The degradation efficiency increased with increasing the amounts up to 0.4 mg/mL, and then the efficiency was nearly stable for both dyes. The increase in the efficiency seems to be due to the increase in the total surface area, namely number of active sites, available for the photocatalytic reaction as the dosage of photocatalyst increased. However, when photocatalyst was overdosed, the number of active sites on the photocatalyst surface may become almost constant because of the decreased light penetration, the increased light scattering and the loss in surface area occasioned by agglomeration (particle–particle interactions) at high solid concentration [47]. Similar trends were reported previously in other photocatalytic reactions over 0.4 mg/mL catalyst [48]. Therefore,

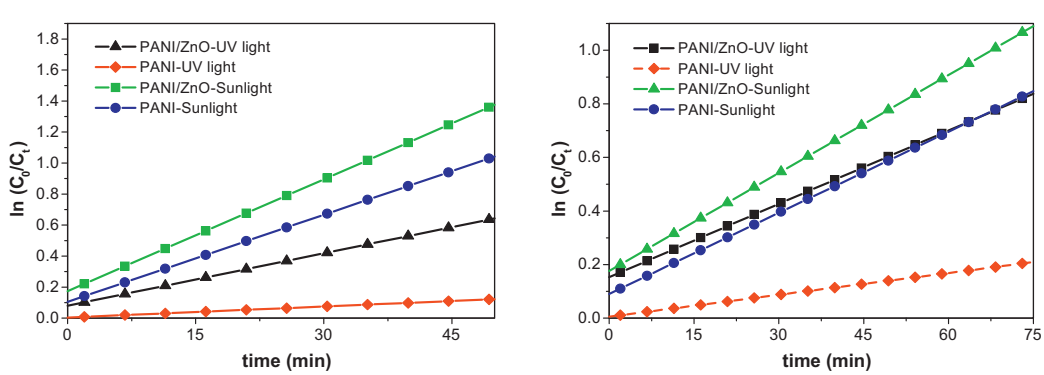


**Fig. 8.** Comparison of the apparent rate constants of MB and MG dyes in the presence of PANI and PANI/ZnO nanocomposite photocatalysts under UV and natural sunlight irradiations (**a**) MB dye and (**b**) MG dye (catalyst concentration: 0.4 mg/mL; initial concentration of dyes: $1 \times 10^{-5}$ M).

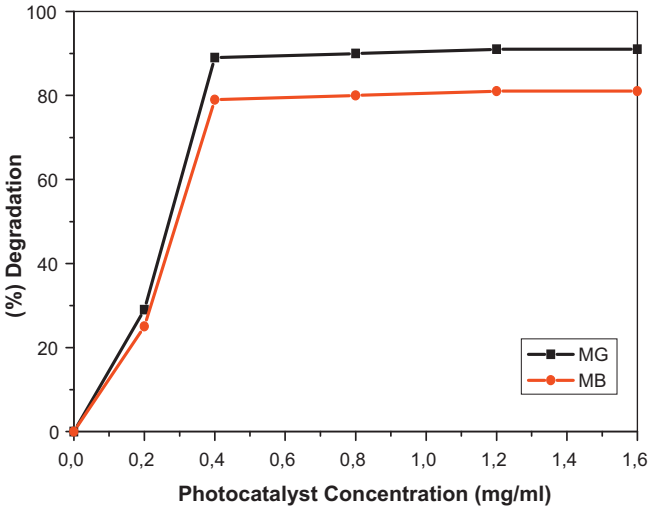


**Fig. 9.** The effect of photo catalyst concentration on degradation of MB and Mg dyes under UV light irradiation after 5 h (initial concentration of dyes: $1 \times 10^{-5}$ M).

0.4 mg mL$^{-1}$ of photocatalyst was selected as the optimal concentration of photocatalyst for the sequential experiment.

### 3.3.3. Photocatalytic stability

To evaluate the photocatalytic stability of the PANI/ZnO nanocomposite, it was used for several photocatalytic runs under UV and natural sunlight irradiations for the both dyes. For this purpose, 1.6 mg/mL of catalyst was added in to the MB or MG solutions ($1 \times 10^{-5}$ M). The same experimental procedure to determine photocatalytic activity as mentioned above was carried out. The concentration changes of dyes were investigated by UV–vis spectroscopic measurements. After measurement, the catalyst was separated from solution by decantation. The separated catalyst was washed with de-ionized water for many times and was dried at 100 °C in air. The dried catalyst was analyzed by FTIR analysis to investigate variation of structure of the catalyst. After FTIR analysis, the catalyst was added into a new ($1 \times 10^{-5}$ M) MB or MG solutions to reuse for photocatalysis experiments. The same experimental procedure was repeated for five times and the concentration change of degradation material and FTIR spectrum of catalyst were recorded for each experiment.

Fig. 10a and c shows the cyclic using of PANI/ZnO nanocomposite for the degradation of the MB and MG dye solution under UV light irradiation, respectively. It has been confirmed that PANI/ZnO nanocomposite continues to maintain good photocatalytic activity also after three cycles. Otherwise, the photocatalytic activity of the PANI/ZnO nanocomposites decreases with the increasing number of cycles.

Fig. 10b and d shows the cyclic using of PANI/ZnO nanocomposite for the degradation of the MB and MG dye solution under natural sunlight irradiation, respectively. It has been confirmed that PANI/ZnO nanocomposite continues to maintain good photocatalytic activity also after five cycles. The degradation rate of the MB dye solution is 95% in the first cycle in the presence of the PANI/ZnO nanocomposite and it takes 240 min, while 82% of the concentration of the MB dye solution degraded in the fifth cycle and this degradation process takes 420 min.

FT-IR analyzes were carried out to confirm the photocatalytic stability of the PANI and the PANI/ZnO nanocomposite after photocatalytic reaction. As seen in Fig. 11, the similarity between the PANI spectrum and the PANI/ZnO nanocomposite spectrum before and after photocatalytic degradation of the MB and MG dyes is clear. It is clear that the structure of the PANI and the PANI/ZnO nanocomposite were not affected during photocatalytic process or were not chemically transformed to other organic compounds.

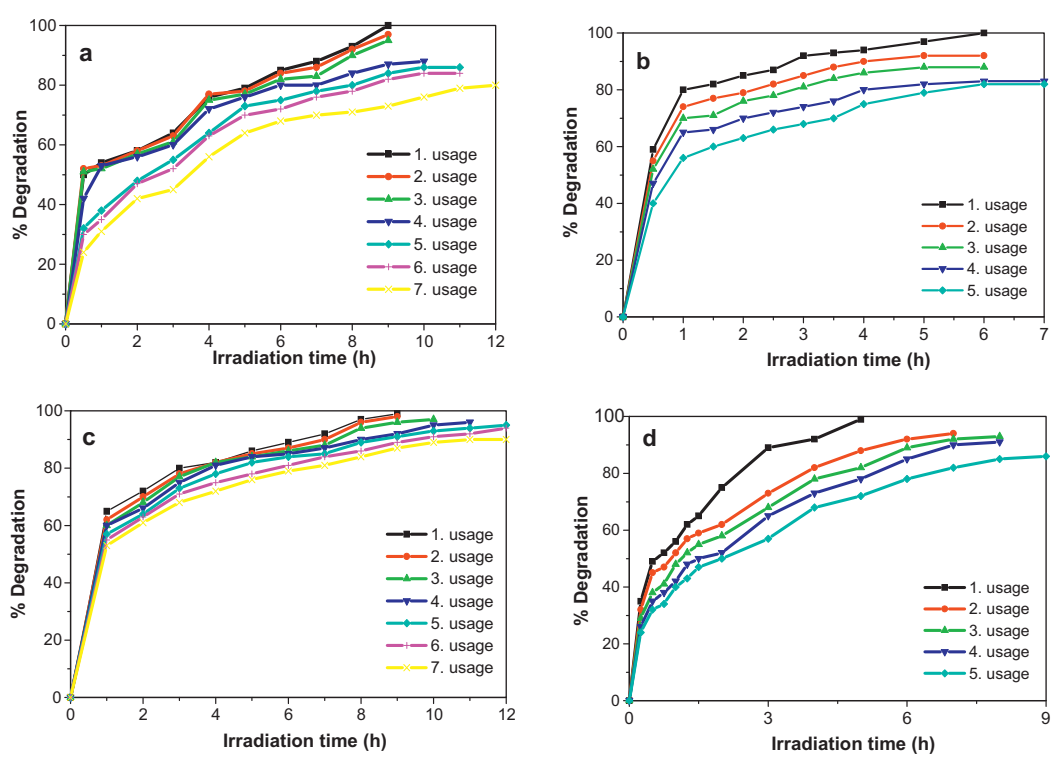


**Fig. 10.** Effect of number of runs on the degradation of dyes in the presence PANI/ZnO nanocomposite (**a**) UV light irradiation of MB, (**b**) natural sunlight irradiation of MB, (**c**) UV light irradiation of MG and (**d**) natural sunlight irradiation of MG (catalyst concentration: 0.4 mg/mL; initial concentration of dyes: $1 \times 10^{-5}$ M).

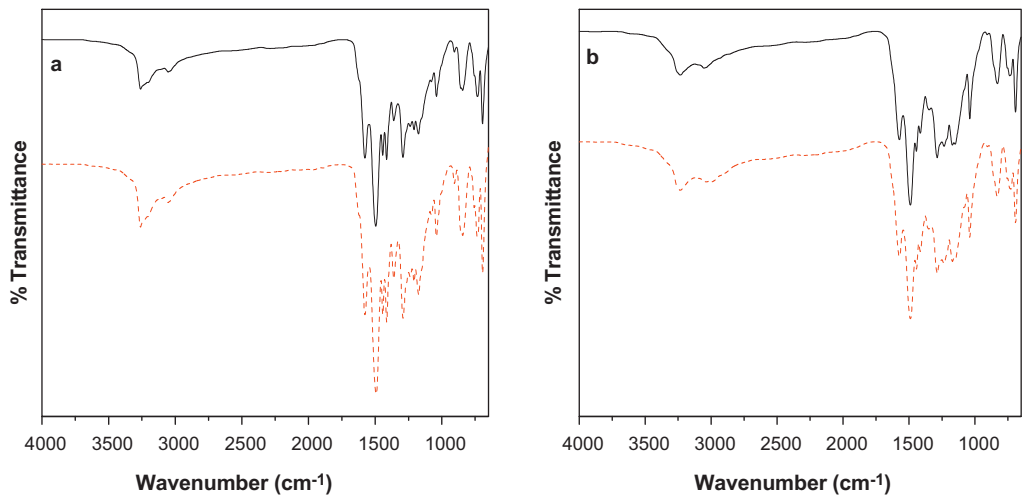


**Fig. 11.** FT-IR spectra of (**a**) PANI and (**b**) PANI/ZnO nanocomposite after photocatalytic reaction in Methylene Blue (black line) and in Malachite green (red line), (catalyst concentration: 0.4 mg/mL; initial concentration of dyes: $1 \times 10^{-5}$ M). (For interpretation of the references to color in this figure legend, the reader is referred to the web version of the article.)

## 4. Conclusions

In summary, the PANI polymer and the PANI/ZnO nanocomposites have been successfully prepared via a facile chemical polymerization method. ZnO nanoparticles were successfully coated with PANI through 'in situ' chemical oxidative polymerization of aniline. The results of FTIR and UV–vis confirm that there is a strong interaction between PANI and ZnO nanoparticles. The nanocomposite particles exhibited a good photocatalytic effect on MB and MG dyes degradation under natural sunlight irradiation. The superior photocatalytic effect of the PANI/ZnO nanocomposites is attributed to the synergistic effect between PANI and ZnO which promotes migration efficiency of the photogenerated carriers on the PANI–ZnO interface. The proposed method may be used for the synthesis of ZnO nanocomposites with various conducting polymer. Overall, conducting polymer-sensitized ZnO composites present a promising method for addressing environmental pollution. Also, the nanocomposite photocatalysts have good photocatalytic stability and can be reused five times with only gradual loss of activity. Thus, the PANI/ZnO nanocomposites are efficient photocatalytic materials for degrading contaminated colored wastewater for reuse in textile industries under mild conditions.

## Acknowledgments

The authors thank Selcuk University Council of Scientific Research Projects for their financial support (Project no: 09401047).

## References

[1] S. Sarmah, A. Kumar, Indian J. Phys. 85 (2011) 713–726.
[2] http://www.methylene-blue.com/substance.php.
[3] V. Adams, J. Marley, Br. Dent. J. 203 (2007) 585–591.
[4] A.J. Linz, R.K. Greenham, L.F. Fallon, J. Occup. Environ. Med. 48 (2006) 523–530.
[5] D.P. Singh, Sci. Adv. Mater. 2 (2010) 245–272.
[6] S.S. Ray, M. Biswas, Synth. Met. 108 (2000) 231–236.
[7] S. Ameen, M.S. Akhtar, Y.S. Kim, O. Yang, H. Shin, Colloid Polym. Sci. 289 (2011) 415–421.
[8] R. Saravanan, H. Shankar, T. Prakash, V. Narayanan, A. Stephen, Mater. Chem. Phys. 125 (2011) 277–280.
[9] K. Gupta, P.C. Jana, A.K. Meikap, J. Appl. Phys. 109 (2011), 123713/1-123713/9.
[10] S. Ameen, M.S. Akhtar, S.G. Ansari, O. Yang, H. Shin, Superlattices Microstruct. 46 (2009) 872–880.
[11] B.K. Sharma, A.K. Gupta, N. Khare, S.K. Dhawan, H.C. Gupta, Synth. Met. 159 (2009) 391–395.
[12] M. Shaolin, K. Jinqing, Synth. Met. 132 (2002) 29–33.
[13] Z. Mandic, L. Duic, J. Electroanal. Chem. 403 (1996) 133–141.
[14] S. Ferrere, A. Zaban, B.A. Gregg, J. Phys. Chem. B 101 (1997) 4490–4493.
[15] S.E. Shaheen, C.J. Brabec, F. Padinger, T. Fromherz, J.C. Hummelen, N.S. Sarıçiftçi, Appl. Phys. Lett. 78 (2001) 841–843.
[16] Z.M. Mbhele, M.G. Sakmane, C.G.C.E. van Sittert, J.M. Nedeljkovic, V. Djokovic, A.S. Luyt, Chem. Mater. 15 (2003) 5019–5024.
[17] M.R. Karim, C.J. Lee, Y.T. Park, M.S. Lee, J. Polym. Chem. 14 (2006) 5283–5290.
[18] Z. Zhang, M. Han, J. Mater. Chem. 13 (2003) 641–643.
[19] P.K. Khanna, S. Lonker, V.S. Subbarao, K.W. Jun, Mater. Chem. Phys. 87 (2004) 49–52.
[20] Ü. Özgür, Y.I. Alivov, C. Liu, A. Teke, M.A. Reshchikov, S. Doğan, V. Avrutin, S.-J. Cho, H. Morkoç, J. Appl. Phys. 98 (2005), 041301/1-041301/100.
[21] H.S. Bae, M.H. Yoon, J.H. Kim, S. Im, Appl. Phys. Lett. 83 (2003) 5313–5315.
[22] F.C.M. Van de pol, Ceram. Bull. 69 (1990) 1959–1965.
[23] Z.C. Jin, I. Hamberg, C.G. Granqvist, B.E. Sernelius, K.-F. Berggren, Thin Solid Films 164 (1988) 381–386.
[24] L. Spanhel, M.A. Anderson, J. Am. Chem. Soc. 113 (1991) 2826–2833.
[25] G. Gustafsson, Y. Cao, G.M. Treacy, F. Klavetter, N. Colaneri, A. Heeger, Nature 357 (1992) 477–479.
[26] M.J. Sailor, E.J. Ginsburg, C.B. Gorman, A. Kumar, R.H. Grubbs, N.S. Lewis, Science 249 (1990) 1146–1149.
[27] R. Gangopadhyay, A. De, Chem. Mater. 12 (2000) 608–622.
[28] M. Zhang, S.L. Fang, A.A. Zakhidov, S.B. Lee, A.E. Aliev, C.D. Williams, K.R. Atkinson, R.H. Baughman, Science 309 (2005) 1215–1219.
[29] K. Lee, Z. Wu, Z. Chen, F. Ren, S.J. Pearton, A.G. Rinzler, Nano Lett. 4 (2004) 911–914.
[30] M. Chang, X.L. Cao, H. Zheng, L. Zhang, Chem. Phys. Lett. 446 (2007) 370–373.
[31] J.P. Pouget, C.H. Hsu, A.G. MacDiarmid, A.J. Epstein, Synth. Met. 69 (1995) 119–120.
[32] S. Min, F. Wang, Y. Han, J. Mater. Sci. 42 (2007) 9966–9972.
[33] W. Feng, E. Sun, A. Fujii, H. Wu, K. Nihara, K. Yoshino, Bull. Chem. Soc. Jpn. 73 (2000) 2627–2633.
[34] M.A. Salem, A.F. Al-Ghonemiy, A.B. Zaki, Appl. Catal. B: Environ. 91 (2009) 59–66.
[35] J. Xu, W. Liu, H. Li, Mater. Sci. Eng. C 25 (2005) 444–447.
[36] F. Fang, J. Futter, A. Markwitz, J. Kennedy, Nanotechnology 20 (2009), 245502/1-245502/7.
[37] W. Zheng, M. Angelopoulos, A.J. Epstein, A.G. McDiarmid, Macromolecules 30 (1997) 2953–2955.
[38] P.R. Somani, R. marimuthu, U.P. Mulik, S.R. Sainkar, D.P. Amelnerkar, Synth. Met. 106 (1999) 45–52.
[39] Z. Niu, Z. Yang, Z. Hu, Y. Lu, C.C. Han, Adv. Funct. Mater. 13 (2003) 949–954.
[40] X. Wang, Y. Li, Y. Zhao, J. Liu, T. Saide, W. Feng, Synth. Met. 160 (2010) 2008–2014.
[41] I. Sedenkova, M. Trchova, J. Stejskal, Polym. Degrad. Stab. 93 (2008) 2147–2157.
[42] Z.X. Xu, V.A.L. Roy, P. Stallinga, M. Muccini, S. Toffanin, H.F. Xiang, C.M. Che, Appl. Phys. Lett. 90 (2007), 223509/1-223509/3.
[43] X. Li, D. Wang, G. Cheng, Q. Luo, J. An, Y. Wang, Appl. Catal. B: Environ. 81 (2008) 267–273.

[44] Q. Li, C. Zhang, J. Li, Appl. Surf. Sci. 257 (2010) 944–948.
[45] S.X. Xiong, Q. Wang, H.S. Xia, Synth. Met. 146 (2004) 37–42.
[46] L.X. Zhang, P. Liu, Z.X. Su, Polym. Degrad. Stab. 91 (2006) 2213–2219.
[47] C.C. Wong, W. Chu, Chemosphere 50 (2003) 981–987.
[48] R.W. Matthews, Water Res. 24 (1990) 653–660.
[49] J.I. Pankove, Optical Processes in Semiconductors, Prentice-Hall, Englewood Cliffs, New Jersey, 1971.
[50] Y. Liu, Y. Ohko, R. Zhang, Y. Yang, Z. Zhang, Hazard. Mater. J. 184 (2010) 386–391.
[51] R. Vinu, S. Polisetti, G. Madras, Chem. Eng. J. 165 (2010) 784–797.
[52] W. Zhao, Z. Bai, A. Ren, B. Guo, C. Wu, Appl. Surf. Sci. 256 (2010) 3493–3498.